

Comparison of IPDA lidar receiver sensitivity for coherent detection and for direct detection using sine-wave and pulsed modulation

Xiaoli Sun^{1,*} and James B. Abshire¹

¹NASA Goddard Space Flight Center, Code 690, Greenbelt, Maryland 20771, USA

*xiaoli.sun-1@nasa.gov

Abstract: We use theoretical models to compare the receiver signal to noise ratio (SNR) vs. average rate of detected signal photons for an integrated path differential absorption (IPDA) lidar using coherent detection with continuous wave (CW) lasers and direct detection with sine-wave and pulse modulations. The results show the coherent IPDA lidar has high receiver gain and narrow bandwidth to overcome the effects of detector circuit noise and background light, but the actual receiver performance can be limited by the coherent mixing efficiency, speckle and other factors. For direct detection, using sine-wave modulation allows the use of a low peak power laser transmitter and synchronous detection. The pulse modulation technique requires higher laser peak powers but is more efficient than sine-wave modulation in terms of average detected signal photon rate required to achieve a given receiver SNR. We also conducted experiments for the direct detection cases and the results agreed well with theory.

©2012 Optical Society of America

OCIS codes: (280.3640) Lidar; (280.1910) DIAL, differential absorption lidar.

References and links

1. R. M. Measures, *Laser Remote Sensing, Fundamentals and Applications* (Krieger, 1992).
2. M. S. Shumate, R. T. Menzies, W. B. Grant, and D. S. McDougal, "Laser absorption spectrometer: remote measurement of tropospheric ozone," *Appl. Opt.* **20**(4), 545–553 (1981).
3. G. N. Pearson and C. G. Collier, "A pulsed coherent CO₂ lidar for boundary-layer meteorology," *Q. J. Roy Meteor Soc. A* **125**, 2703–2721 (1999).
4. G. J. Koch, B. W. Barnes, M. Petros, J. Y. Beyon, F. Amzajerjian, J. Yu, R. E. Davis, S. Ismail, S. Vay, M. J. Kavaya, and U. N. Singh, "Coherent differential absorption lidar measurements of CO₂," *Appl. Opt.* **43**(26), 5092–5099 (2004).
5. F. Gibert, P. H. Flamant, D. Bruneau, and C. Loth, "Two-micrometer heterodyne differential absorption lidar measurements of the atmospheric CO₂ mixing ratio in the boundary layer," *Appl. Opt.* **45**(18), 4448–4458 (2006).
6. F. Gibert, P. H. Flamant, J. Cuesta, and D. Bruneau, "Vertical 2-um heterodyne differential absorption Lidar measurements of mean CO₂ mixing ratio in the troposphere," *J. Atmos. Ocean. Technol.* **25**(9), 1477–1497 (2008).
7. G. D. Spiers, R. T. Menzies, J. Jacob, L. E. Christensen, M. W. Phillips, Y. Choi, and E. V. Browell, "Atmospheric CO₂ measurements with a 2 μm airborne laser absorption spectrometer employing coherent detection," *Appl. Opt.* **50**(14), 2098–2111 (2011).
8. J. Pruitt, M. E. Dobbs, M. Gypson, B. R. Neff, and W. E. Sharp, "High-speed CW lidar retrieval using spectral lock-in algorithm," *Proc. SPIE* **5154**, 138–145 (2003).
9. M. Dobbs, J. Pruitt, N. Blume, D. Gregory, and W. Sharp, "Matched filter enhanced fiber-based lidar for earth, weather and exploration," 6th Annual NASA Earth Science Technology Conference (ESTF), 27–29 June, College Park, MD, Paper B4P3 (2006).
10. S. Kameyama, M. Imaki, Y. Hirano, S. Ueno, S. Kawakami, D. Sakaizawa, and M. Nakajima, "Development of 1.6 microm continuous-wave modulation hard-target differential absorption lidar system for CO₂ sensing," *Opt. Lett.* **34**(10), 1513–1515 (2009).
11. J. Caron, Y. Durand, J. Bezy, and R. Meynart, "Performance modeling for A-SCOPE: a space borne lidar measuring atmospheric CO₂," *Proc. SPIE* **7479**, 74790E (2009).

12. J. B. Abshire, H. Riris, G. R. Allan, C. J. Weaver, J. Mao, X. Sun, W. E. Hasselbrack, S. R. Kawa, and S. Biraud, "Pulsed airborne lidar measurements of atmospheric CO₂ column absorption," *Tellus B Chem. Phys. Meteorol.* **62**(5), 770–783 (2010).
 13. J. W. Goodman, "Statistical properties of laser speckle patterns," in *Laser Speckle and Related Phenomena*, J. C. Dainty ed. (Springer-Verlag, 1975).
 14. C. S. Gardner, "Target signatures for laser altimeters: an analysis," *Appl. Opt.* **21**(3), 448–453 (1982).
 15. P. H. Flamant, R. T. Menzies, and M. J. Kavaya, "Evidence for speckle effects on pulsed CO₂ lidar signal returns from remote targets," *Appl. Opt.* **23**(9), 1412–1417 (1984).
 16. R. M. Gagliardi and S. Karp, *Optical Communications*, 2nd ed. (John Wiley and Sons, 1995).
 17. R. N. McDonough and A. D. Whalen, *Detection of Signal in Noise*, 2nd ed. (Academic Press, 1995)
-

1. Introduction

Integrated path differential absorption (IPDA) lidar may be used to remotely measure the average gas molecular density in the path of the laser beam to a hard target [1]. The typical two-wavelength approach uses one laser with the wavelength locked to the gas absorption line (on-line), and the other to a nearby absorption free region (off-line). The molecular density of the gas can be derived from the ratio of the normalized energies in the laser echo signals at the on-line and off-line wavelengths if the path length, temperature and pressure are known.

IPDA lidar was first used from aircraft for the remote sensing of ozone (O₃) [2]. The technique has also been used to measure column CO₂ and CH₄ concentrations from aircraft [3–12]. Recently investigators have conducted airborne experiments using IPDA lidar based on coherent detection using continuous wave (CW) lasers, and direct detection using sine-wave modulation and pulse modulation. Each approach may have advantages and disadvantages in measurement performance, system complexity, laser availability, etc., depending on the application.

Our objective for this work was to identify IPDA lidar approaches that are attractive for space-based use, such as the CO₂ lidar for NASA's planned Active Sensing of CO₂ Emission over Nights, Days, and Seasons (ASCENDS) mission. For space lidar, the signal scattering losses are usually high due to the long range to the surface and the instrument size, mass, and power are limited due their impact on costs. Therefore a typical goal for space-based lidar design is to minimize the product of the average transmitted laser power and receiver telescope area to achieve a given receiver signal to noise ratio (SNR). Here we analyze three different laser modulation and detection techniques for IPDA lidar to determine how the receiver SNR depends on average received laser signal power, and show the results of supporting experiments.

2. IPDA lidar approaches

2.1. Coherent IPDA lidar

Coherent lidar have been studied extensively and some examples are given in References [3–7]. A laser transmitter for a typical coherent IPDA lidar consists of two seed lasers, one on-line and one off-line, followed by a laser power amplifier, as shown in Fig. 1. The laser transmitter in a coherent IPDA lidar can be either a CW or a pulsed laser. The former has the advantage of low peak power and ease of maintaining coherence between the transmitted and the received signal, but the latter can provide range resolved measurements.

Figure 2 shows a block diagram of a coherent IPDA lidar receiver. The local oscillator signal can be derived from the laser transmitter via the use of a beam splitter. The photodetector is a square-law device and produces the difference (carrier) frequency signal, as in a radio frequency (RF) heterodyne receiver. An electrical band-pass filter (BPF) is used after the detector to select only the signal at the carrier frequency. For IPDA lidar, the relevant signal is the amplitude squared of the down-converted sinusoidal carrier signal so that it is proportional of the intensity of the reflected laser signal. This can be obtained with several techniques, such as the conventional approach shown in Fig. 2. Spiers [7] recently

reported an airborne IPDA lidar using a digital signal processing technique in which the signal waveform was first digitized and a Fast Fourier Transform (FFT) was used to detect and estimate the power of the heterodyne carrier signal from the FFT spectrum.

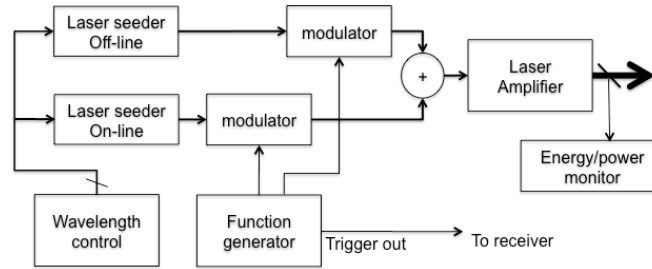


Fig. 1. Block diagram of a IPDA lidar transmitter. For a coherent IPDA lidar, the laser can be modulated in phase, frequency, amplitude, or not modulated in the case of a CW lidar. For a direct detection lock-in type IPDA lidar, the lasers are intensity modulated with sine-waves of known frequencies. For a direction detection pulsed IPDA lidar, the lasers are intensity modulated with a pulse train.

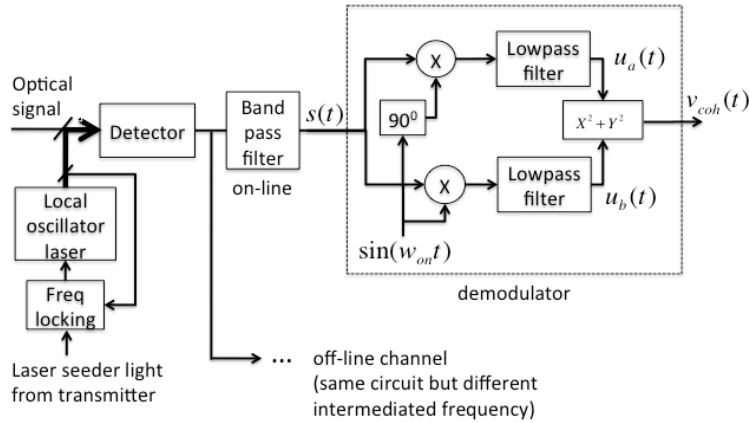


Fig. 2. Block diagram of a coherent IPDA lidar receiver. The local oscillator laser can be obtained by splitting a small portion of the transmitted laser light. The sinusoidal signal amplitude estimator shown in the dotted box is an example following the conventional RF approach. The same function may be carried out using different techniques, such as FFT followed by a peak-detection as described in [7].

There are several advantages of using coherent techniques for IPDA lidar. The heterodyne process uses the local oscillator to effectively amplify the received signal to override the circuit noise and achieve a nearly quantum-limited performance. The detector output of a coherent lidar is linear with the electro-magnetic field of the received laser signal but is shifted to a RF carrier frequency. One can directly measure the phase and the frequency of the received optical signal to obtain full information about the target, including Doppler shift. The receiver's optical bandwidth is defined by the bandwidth of the RF BPF, which can be several orders of magnitude narrower than that of a narrow-band optical filter. As a result, a coherent lidar can operate with much higher background light than a direct detection lidar.

However, using a coherent technique also brings in several constraints. It requires a high degree of coherence between the local oscillator and the received signal in temporal and spatial modes and polarization. It requires the use of single mode lasers with sufficient frequency and phase stability, and diffraction-limited optics. It can be sensitive to environment factors, such as vibration and thermal expansion at the scale of a wavelength. The overall receiver performance is often limited by the coherent mixing efficiency.

Laser speckle also imposes a major constraint. Speckle effects arise from the coherent interference of the laser light reflected from a rough target, which is characteristic of an airborne or space borne lidar [13–15]. The wave-front of the received laser light is no longer a plane wave but has complex spatial structure. The received signal level varies with the random phase distribution of the backscatter, which changes as the spacecraft travels and illuminates different ground targets. The average size of laser speckle cells at the receiver can be approximated as $R\lambda/d_{laser}$ [13] with R the range to the target, λ the laser wavelength, and d_{laser} the diameter of the laser footprint size on ground, which can be written as $d_{laser} = 2.44 R\lambda/D_{Xmit}$ with D_{Xmit} the diameter of the laser beam transmitter. To maintain a reasonable mixing efficiency, the receiver telescope diameter needs to be comparable to the average speckle size, or about the same size as the laser transmitter. It is desirable in practice to increase the receiver telescope size to collect more signals without increasing the laser power. But for coherent lidar, the size of the transmitted laser beam has to be increased with the receiver telescope size, which in turn affects the laser beam divergence angle, footprint size on ground, and spatial averaging for measurements from a moving platform.

2.2. Direct detection

A direct detection IPDA lidar measures the energy or power of the received optical signal. It does not have a local oscillator laser and the associated complexity in maintaining coherence between the transmitted and the received signal. The receiver telescope diameter is usually chosen to be many times the average laser speckle size to allow spatial averaging of the speckle noise and to collect more signal photons without increasing the laser power. Due to these factors, a direct detection lidar usually costs less to build for use in space. However, the receiver performance is limited by the detector quantum efficiency, detector dark noise and circuit noise. Since the receiver's optical band-pass is orders of magnitude wider than that of a coherent lidar, background light is usually a significant noise source for daytime operation.

To date, investigators have mainly used two types of signaling techniques for direct detection IPDA lidars. The first technique uses sine-wave laser intensity modulation. Typically two CW seeder lasers (on-line and off-line) are used, each is intensity modulated by a sine-wave (subcarrier) at a given frequency, and the sum of the two is amplified and transmitted to the targets. The receiver uses synchronous detection to retrieve the subcarrier signals through a narrow BPF centered at the subcarrier frequency [8–10], as shown in Fig. 3. The receiver approach is sometimes called lock-in detection.

Unlike coherent lidars, the signal output from the photodetector varies linearly with the intensity of the received laser signal and the measurement is the amplitude of the sinusoidal subcarrier signal. The noise from background light is proportional to the optical BPF bandwidth. The approach can be extended in wavelength by adding additional seed lasers, subcarrier frequencies and lock-in receiver channels. It is also possible to estimate the target range by periodically sweeping the subcarrier frequency in a similar fashion as a frequency-modulated (FM) radar.

One advantage of the sine-wave modulated approach is that the transmitter operates in a quasi CW mode with the peak power always equal to twice the average power. The on-line and off-line lasers can be operated simultaneously and the signals can be separated in the receiver as long as the on-line and off-line laser modulation frequencies are sufficiently separated. The receiver can use conventional lock-in electronics.

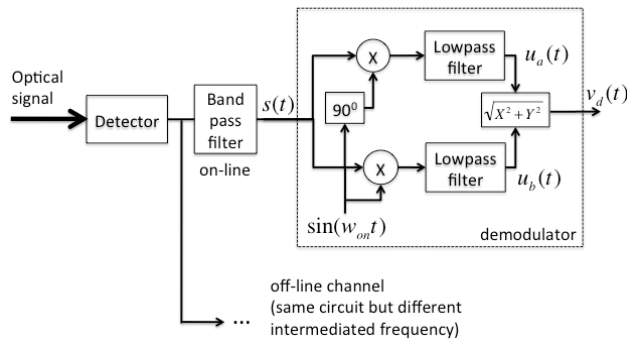


Fig. 3. Receiver block diagram of a direct detection sine-wave modulation IPDA lidar.

A sine-wave modulated direction IPDA lidar is more susceptible to background light than a coherent IPDA lidar because the receiver's noise bandwidth is defined by its wider optical bandpass. The receiver has to integrate both the signal and background noise continuously in time without a range gate. It is also difficult to measure surface reflections through thin clouds or aerosol layers, even with FM lidar techniques.

The other type of direct detection IPDA lidar uses lasers with much higher peak powers but pulsed at a low duty cycle, with the laser pulses alternating between the on-line and off-line wavelengths [11,12]. Figure 4 shows a comparison of the laser output waveforms from a sine-wave modulated and a pulse modulated IPDA lidar.

The pulsed IPDA lidar receiver uses a single photon detector followed by a photon histogrammer, or a waveform recorder in the case of analog photodetector, to record the time resolved signals for each wavelength, as shown in Fig. 5. It provides not only the time (range) resolved surface returns but also atmosphere backscatter profiles in the laser beam path. The receiver integrates the signal only within a narrow time interval (or range gate) about the echo pulse from the target. This eliminates the effect of atmosphere scattering in IPDA measurement and greatly reduces the effects of solar background and detector dark noise.

A disadvantage of pulsed approach is the higher peak powers and low duty cycles, which is not optimum for some laser types. For space-based measurements through Earth's atmosphere, the laser pulse rate is limited to ~8 kHz, so that there is only one laser pulse at a time propagating through the primary scattering depth of the atmosphere (typically ~19 km to the surface).

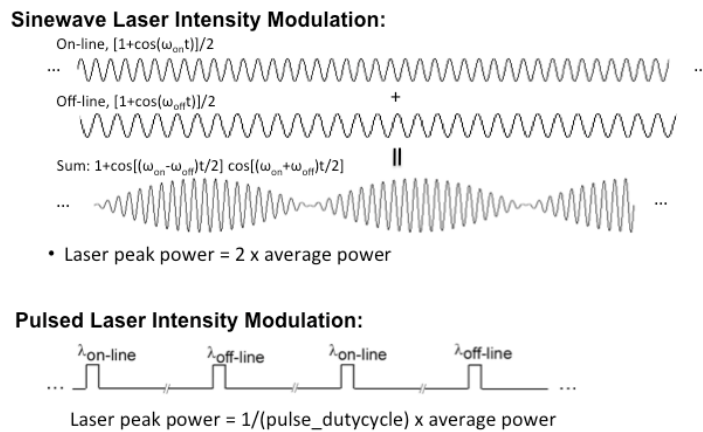


Fig. 4. Laser output waveforms of sine-wave modulation and pulsed modulation IPDA lidar.

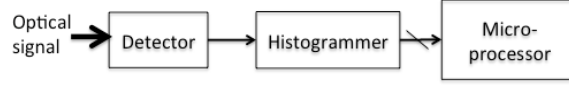


Fig. 5. Receiver block diagram for a direct detection photon counting pulsed modulation IPDA lidar.

3. Receiver SNR comparison–Theory

3.1. Coherent CW IPDA lidar

For a coherent CW IPDA lidar, the receiver SNR for either on-line or off-line wavelength measurement can be defined as the ratio of the mean to standard deviation of the power of the subcarrier signal output from the demodulator shown in Fig. 2. Here we assume measurements from a moving platform with an off-nadir pointed laser beam, so the Doppler shift of the received laser signal naturally forms a difference frequency signal for the heterodyne detection, as in [7]. We also assume that the received laser signal power is equally split among on-line and off-line wavelength. In practice, there is more absorption at the on-line wavelength but one can pre-compensate it by splitting more laser power into the on-line wavelength at the transmitter. The on-line signal output from the BPF, $s(t)$, as indicated in Fig. 2, can be expressed as

$$s(t) = \langle s(t) \rangle + \varepsilon(t) \quad (1)$$

where $\langle s(t) \rangle$ is the average signal and $\varepsilon \equiv s(t) - \langle s(t) \rangle$ is the noise. The average signal is given by

$$\langle s(t) \rangle = A_{on} \cos(\omega_{on} t + \phi_{on}) \quad (2)$$

with A_{on} , ω_{on} , and ϕ_{on} the amplitude, frequency, and phase of the sinusoidal heterodyne carrier signal. The noise can be modeled as a band-limited white noise centered at ω_{on} .

Following the mathematical models derived by Gargaliardi and Karp for laser communications [16], the amplitude of the sinusoidal signal and the one-sided noise spectral density can be expressed as

$$A_{on} = 2 \frac{\eta_{det}}{hf} \eta_c q \sqrt{\frac{\langle P_{sig} \rangle}{2}} \sqrt{P_{LO}}, \quad (3)$$

$$N_n = 2 \left[\frac{\eta_{det}}{hf} q^2 P_{LO} + \left(\frac{\eta_{det}}{hf} q P_{LO} \right) \left(\frac{\eta_{det}}{hf} q N_{bg} \right) + N_{cir} \right]. \quad (4)$$

Here η_{det} is the detector quantum efficiency, hf is the photon energy, η_c is the coherent mixing efficiency (or the fraction of the received signal and the local oscillator laser that are matched exactly in spatial and longitudinal modes and polarizations), q is the electron charge, $\langle P_{sig} \rangle$ is the average power of the received laser signal split among the on-line and off-line wavelength components, P_{LO} is the power of the local oscillator laser, N_{bg} is the power spectral density of the background light in unit of W/Hz , and N_{cir} is the circuit noise spectral density in unit of A^2/Hz .

The signal from the upper quadrature channel after the low-pass filter (LPF), $u_a(t)$, as shown in Fig. 2, can be written as,

$$\begin{aligned}
u_a(t) &= \left\{ \left[A_{on} \cos(\omega_{on}t + \phi_{on}) + \varepsilon(t) \right] \cos(\omega_{on}t) \right\} * h_{LPF}(t) \\
&= \frac{A_{on}}{2} \cos(\phi_{on}) + \left[\varepsilon(t) \cos(\omega_{on}t) \right] * h_{LPF}(t)
\end{aligned} \tag{5}$$

where “ $*$ ” represents the convolution operator and $h_{LPF}(t)$ represents the LPF impulse response that satisfies $\int_{-\infty}^{\infty} h_{LPF}(t) dt \equiv 1$. It is assumed the LPF bandwidth is sufficiently narrow that it can filter out all signal and noise at the second harmonics of the carrier frequency. Similar to Eq. (5), the signal from the lower quadrature channel can be written as,

$$\begin{aligned}
u_b(t) &= \left\{ \left[A_{on} \cos(\omega_{on}t + \phi_{on}) + \varepsilon(t) \right] \sin(\omega_{on}t) \right\} * h_{LPF}(t) \\
&= -\frac{A_{on}}{2} \sin(\phi_{on}) + \left[\varepsilon(t) \sin(\omega_{on}t) \right] * h_{LPF}(t).
\end{aligned} \tag{6}$$

The signal after the sum of squares, as indicated in Fig. 2, becomes

$$\begin{aligned}
v_{coh}(t) &= u_a^2(t) + u_b^2(t) \\
&= \left(\frac{A_{on}}{2} \right)^2 + 2 \frac{A_{on}}{2} \left[\varepsilon(t) (\cos(\omega_{on}t) \cos(\phi_{on}) - \sin(\omega_{on}t) \sin(\phi_{on})) \right] * h_{LPF}(t) \\
&\quad + \left[(\varepsilon(t) \cos(\omega_{on}t)) * h_{LPF}(t) \right]^2 + \left[(\varepsilon(t) \sin(\omega_{on}t)) * h_{LPF}(t) \right]^2.
\end{aligned} \tag{7}$$

The average of the demodulated signal can now be written as

$$\mu_{coh} = \langle v_{coh}(t) \rangle = \left(\frac{A_{on}}{2} \right)^2 + \left\langle \left[(\varepsilon(t) \cos(\omega_{on}t)) * h_{LPF}(t) \right]^2 \right\rangle + \left\langle \left[(\varepsilon(t) \sin(\omega_{on}t)) * h_{LPF}(t) \right]^2 \right\rangle \tag{8}$$

Note there is a positive bias due to the sum of squares operation in the carrier demodulator.

Since the noise $\varepsilon(t)$ is narrow band and centered at the carrier frequency, it can be expressed as the sum of two quadrature components [17], as

$$\varepsilon(t) = \varepsilon_c(t) \cos(\omega_{on}t) + \varepsilon_s(t) \sin(\omega_{on}t) \tag{9}$$

where $\varepsilon_c(t)$ and $\varepsilon_s(t)$ are the in-phase and quadrature components near DC (zero frequency). The two-sided power spectra of the two noise components, $N_c(\omega)$ and $N_s(\omega)$, can be written in terms of that of the total noise, $N(\omega)$, as [17]

$$N_c(\omega) = N_s(\omega) = \left[N(\omega - \omega_{on}) + N(\omega + \omega_{on}) \right]. \tag{10}$$

The second term in Eq. (8) becomes

$$\begin{aligned}
\sigma_c^2 &= \left\langle \left[(\varepsilon(t) \cos(\omega_{on}t)) * h_{LPF}(t) \right]^2 \right\rangle \\
&= \left\langle \left[\left((\varepsilon_c(t) \cos(\omega_{on}t) + \varepsilon_s(t) \sin(\omega_{on}t)) \cos(\omega_{on}t) \right) * h_{LPF}(t) \right]^2 \right\rangle \\
&= \left\langle \left[\frac{1}{2} \varepsilon_c(t) * h_{LPF}(t) \right]^2 \right\rangle \\
&= \left(\frac{1}{2} \right)^2 \frac{1}{2\pi} \int_{-\infty}^{\infty} N_c(\omega) |H_{LPF}(\omega)|^2 d\omega.
\end{aligned} \tag{11}$$

For narrow-band white noise, the power spectra for the quadrature noise components can be written as $N_c(\omega) = N_n$ for $|\omega| < 2\pi B_{LPF}$ where N_n is given in Eq. (4) and B_{LPF} is the one-sided noise bandwidth near DC. As a result, Eq. (11) can be simplified to $\sigma_c^2 = N_n B_{LPF} / 2$. Similarly the third term in Eq. (8) can be written as $\sigma_s^2 = \sigma_c^2 = N_n B_{LPF} / 2$.

The average signal, Eq. (8), can now be written as

$$\mu_{coh} = \left(\frac{A_{on}}{2}\right)^2 + N_n B_{LPF} = \left(\frac{A_{on}}{2}\right)^2 \left(1 + \frac{N_n B_{LPF}}{(A_{on}/2)^2}\right). \quad (12)$$

When the SNR is high, $A_{on} \gg |\varepsilon(t)|$, the variance of the signal can be closely approximated by neglecting the last two terms of Eq. (8) and using the results from Eq. (11), as

$$\sigma_{coh}^2 = \langle (v_{coh}(t) - \langle v_{coh}(t) \rangle)^2 \rangle \approx A_{on}^2 \langle [(\varepsilon(t) \cos(\omega_{on} t + \phi_{on})) * h_{LPF}(t)]^2 \rangle = A_{on}^2 \frac{N_n B_{LPF}}{2}. \quad (13)$$

The receiver SNR for coherent IPDA lidar can now be written as

$$SNR_{coh} \equiv \frac{\mu_{coh}}{\sigma_{coh}} \approx \frac{A_{on}}{2\sqrt{2}\sqrt{N_n B_{LPF}}}. \quad (14)$$

The average of the demodulated signal, Eq. (12), can also be expressed in terms of SNR_{coh} , as

$$\mu_{coh} = \left(\frac{A_{on}}{2}\right)^2 \left(1 + \frac{1}{2SNR_{coh}^2}\right). \quad (15)$$

Therefore the relative bias in coherent IPDA lidar measurement due to the sum of square operation is equal to $1/2SNR_{coh}^2$, which can be negligible when the SNR is high.

The IPDA measurements are usually obtained by sampling the LPF output at the integration interval. An ideal LPF should completely reject the second harmonics of the heterodyne carrier signal and have a finite impulse response time so that there is no interference between successive measurements. In practice, a finite time response LPF, such as a box-car type integrator, has wide frequency response and may not completely null the second harmonics of the relatively strong carrier signal, especially for coherent IPDA lidar from a moving platform where the carrier frequency varies with the target slope. A sharp cut-off frequency response LPF, such as a Butterworth LPF, has a long a response time that can span several sampling intervals. Here we choose a Gaussian LPF, which can be approximated closely in practice with a Bessel LPF, and a noise bandwidth that satisfies

$$B_{LPF} \approx \frac{1}{T_s} \quad (16)$$

with T_s the sampling interval.

The SNR for the coherent IPDA lidar can be obtained by substituting Eqs. (3), (4), and Eq. (16) into (14) and assuming the shot noise from the local oscillator laser power is much higher than the circuit noise, yielding,

$$SNR_{coh} = \frac{\eta_c \sqrt{\frac{\eta_{det} \langle P_{sig} \rangle T_s}{hf}}}{2 \sqrt{1 + \left(\frac{\eta_{det}}{hf} q N_{bg} \right)}}. \quad (17)$$

The effect of solar background light can often be neglected with coherent lidar. For example, for the proposed CO₂ lidar for NASA's ASCENDS mission with 1-m diameter receiver aperture size at 450-km spacecraft altitude, the power spectral density for solar background light is $N_{bg} < 1 nW/nm \approx 8.2 \times 10^{-21} W/Hz$, and the detector responsivity is typically $(\eta_{det}/hf)q \approx 1 A/W$ at $1.57 \mu m$ [12]. For this case, $(\eta_{det}/hf)N_{bg} < 0.05$, the solar background noise term in the denominator of Eq. (17) can be neglected, and the receiver SNR can be approximated as

$$SNR_{coh} = \frac{\eta_c}{2} \sqrt{\frac{\langle n_{sig} \rangle}{2}} \quad (18)$$

where we have denoted the average number of detected signal photons over the sampling interval as

$$\langle n_{sig} \rangle \equiv \frac{\eta_{det}}{hf} \langle P_{sig} \rangle T_s. \quad (19)$$

3.2. Sine-wave modulation, direct detection

For the sine-wave modulated direct detection lidar, the signal from the photodetector is a composite with both sinusoidal sub-carrier signals plus noise. The sum of the on-line and off-line laser signals can be written as

$$S_L = \frac{\langle P_{sig} \rangle}{2} \{ [1 + \cos(\omega_{on} t)] + [1 + \cos(\omega_{off} t)] \} \quad (20)$$

where ω_{on} and ω_{off} are the on-line and off-line subcarrier frequencies. The peak power of the combined signal is always equals to one half of the average power.

The signal output from the photodetector in this case is proportional to the laser intensity and the measurement is the root-mean-squares of the two quadrature components, as shown in Fig. 3. The amplitude of the sinusoidal subcarrier signal and the one-sided noise power spectrum are given by [16]

$$A_{on} = \frac{\eta_{det}}{hf} q \frac{\langle P_{sig} \rangle}{2} \quad (21)$$

$$N_n = 2 \left[\frac{\eta_{det}}{hf} q^2 (\langle P_{sig} \rangle + N_{bg} \Delta\lambda) + N_{cir} \right]. \quad (22)$$

Here N_{bg} is the power spectral density of background light in unit of W/nm , and $\Delta\lambda$ is receiver optical bandwidth.

The signal output from the subcarrier demodulator can be derived to a good approximation by taking the first two terms of the power series and following the derivation of Eqs. (7) through (11), as

$$v_d(t) = \sqrt{u_a^2(t) + u_b^2(t)} \approx \frac{A_{on}}{2} \left\{ 1 + \frac{1}{2} \frac{1}{\left(\frac{A_{on}}{2}\right)^2} \left[A_{on} [\varepsilon(t) \cos(\omega_{on} t + \phi_{on})] * h_{LPF}(t) + [(\varepsilon(t) \cos(\omega_{on} t)) * h_{LPF}(t)]^2 + [(\varepsilon(t) \sin(\omega_{on} t)) * h_{LPF}(t)]^2 \right] \right\}. \quad (23)$$

The average signal at the output of the demodulator can be obtained by averaging the right hand side of Eq. (23) and using the result in Eq. (13), yielding,

$$\mu_{sin} = \langle v_d(t) \rangle = \frac{A_{on}}{2} \left(1 + \frac{2N_n B_{LPF}}{A_{on}^2} \right) \approx \frac{A_{on}}{2}. \quad (24)$$

Note there is a positive bias term in the average signal due to the sum of square operation, like in a coherent IPDA lidar, though it is usually negligible under high SNR conditions.

The variance of the signal under high SNR can be derived similarly to Eq. (13), as

$$\sigma_{sin}^2 = \langle [v_d(t) - \langle v_d(t) \rangle]^2 \rangle \approx \langle [(\varepsilon(t) \cos(\omega_{on} t + \phi_{on})) * h_{LPF}(t)]^2 \rangle = \frac{N_n B_{LPF}}{2}. \quad (25)$$

The receiver SNR for the on-line wavelength can now be written by substituting Eqs. (16), (21), (22) into (24) and (25) and taking the ratio of the mean and standard deviation, as

$$SNR_{sin} = \frac{\mu_{sin}}{\sigma_{sin}} = \frac{\frac{1}{2} \frac{\eta_{det}}{hf} q \frac{\langle P_{sig} \rangle}{2}}{\sqrt{2 \left[\frac{\eta_{det}}{hf} q^2 (\langle P_{sig} \rangle + N_{bg} \Delta \lambda) + N_{cir} \right] \frac{1}{2T_s}}} = \frac{\langle n_{sig} \rangle}{4 \sqrt{\langle n_{sig} \rangle + (n'_{bg} + n'_{dark} + n'_{cir}) T_s}} \quad (26)$$

where $\langle n_{sig} \rangle$ is defined by Eq. (19), and $n'_{bg} = (\eta_{det}/hf) P_{bg} \Delta \lambda$, $n'_{dark} = I_{dark}/q$, and $n'_{cir} = N_{cir}/q^2$ are the rates of the background light photons, detector dark noise counts, and equivalent preamplifier circuit noise, respectively. The receiver's bandwidth for the background light in this case is determined by the width of the optical BPF and the solar background light is a significant noise factor.

3.3. Pulsed modulation, direct detection

The signal for a pulsed direct detection IPDA lidar consists of the sum of detected signal photons for all the pulses over the sampling interval at the alternating on-line or off-line wavelengths. There is no intermediate subcarrier signal and the receiver can simply integrate the received pulse energy with a box-car type integrators. The total number of laser pulses at each wavelength is given by $f_{pul} T_s / 2$ where f_{pul} is the pulse rate at on-line or off-line wavelengths.

The average signal in terms of detected photons at each wavelength is given by [12]

$$\mu_{pul} = \left(\frac{f_{pul} T_s}{2} \right) \left(\frac{\eta_{det}}{hf} \langle P_{sig} \rangle \frac{1}{f_{pul}} \right) = \frac{1}{2} \frac{\eta_{det}}{hf} \langle P_{sig} \rangle T_s = \frac{1}{2} \langle n_{sig} \rangle. \quad (27)$$

The standard deviation of the detected signal photons at each wavelength can be written as

$$\begin{aligned}\sigma_{pul} &= \sqrt{\left(\frac{f_{pul} T_s}{2}\right) \left[\frac{\eta_{det} \langle P_{sig} \rangle}{hf f_{pul}} + \left(\frac{\eta_{det} P_{bg} \Delta\lambda}{hf} + \frac{I_{dark}}{q} + \frac{N_{cir}}{q^2} \right) \tau_{pw} \right]} \\ &= \sqrt{\frac{1}{2} \left[\langle n_{sig} \rangle + (n'_{bg} + n'_{dard} + n'_{cir}) T_s \alpha_{duty} \right]}\end{aligned}\quad (28)$$

where τ_{pw} is the laser pulse width and $\alpha_{duty} = f_{pul} \tau_{pw}$ is the laser pulse duty cycle. From Eqs. (27) and (28), the SNR for a single wavelength of the pulsed IPDA lidar can be written as

$$SNR_{pul} = \frac{\mu_{pul}}{\sigma_{pul}} = \frac{\langle n_{sig} \rangle}{\sqrt{2} \sqrt{\langle n_{sig} \rangle + (n'_{bg} + n'_{dard} + n'_{cir}) T_s \alpha_{duty}}}. \quad (29)$$

The receiver SNR has a similar form as Eq. (26) for the sine-wave modulation IPDA lidar but the noises from the solar background light, the detector dark noise and circuit noise are multiplied by the pulse duty factor. Since usually $\alpha_{duty} \ll 1$, the impact of these noise terms is considerably smaller than those for sine-wave modulated IPDA lidar.

3.4. Comparison of the SNR for the different techniques

The expressions for SNR for the single wavelength detection given in Eqs. (18), (26) and (29) can be used to compare the receiver performance assuming they all have the same receiver optical efficiency. Under ideal conditions when the background light and detector dark noise are zero, the detector quantum efficiencies are the same for all three cases, and the coherent mixing efficiency is 100%, the ratios of SNRs for the sine-wave and pulsed modulation lidars to that of the coherent lidar are given by

$$\frac{SNR_{sin}}{SNR_{coh}} \rightarrow \frac{\sqrt{2}}{2} \quad \text{and} \quad \frac{SNR_{pul}}{SNR_{coh}} \rightarrow 2 \quad (30)$$

The SNR for the pulsed IPDA lidar is a factor of 2 higher than that of a coherent lidar. One reason for the differences is the noise bandwidth of the LPF. For coherent and sine-wave modulated IPDA lidar, the LPF has to reject the second harmonics of the relatively strong sinusoidal carrier signals and have an impulse response duration less than the sampling interval of the IPDA measurements. The relationship between noise bandwidth and the receiver integration time is assumed to be $B_{LPF} = 1/T_s$ as in Eq. (16). It may be possible to further reduce the noise bandwidth. For example, a box-car type integrator may be used if the carrier frequency is exactly known and the integration time is set to be an exact multiple of the period of the carrier signal. For pulsed modulation and detection IPDA lidar, there is no a sinusoidal carrier signal or the harmonics and so the LPF can be a simple box-car integrator with a noise bandwidth equal to half that given in Eq. (16).

For the two direct detection cases, one can compare the ratio of single wavelength SNRs at given background light, detector dark noise, and circuit noise from the preamplifier. The result is

$$\frac{SNR_{pul}}{SNR_{sin}} = 2\sqrt{2} \frac{\sqrt{\langle n_{sig} \rangle + (n'_{bg} + n'_{dard} + n'_{cir}) T_s}}{\sqrt{\langle n_{sig} \rangle + (n'_{bg} + n'_{dard} + n'_{cir}) T_s \alpha_{duty}}}. \quad (31)$$

This shows that the receiver SNR of a pulsed lidar is at least $2\sqrt{2}$ times higher than that of a sine-wave modulation lock-in IPDA lidar under the same input signal level. Furthermore, the range gating in the pulsed IPDA receiver blocks out most of the background light noise and the detector dark noise, which improves the SNR under high background light conditions.

The sine-wave modulation with lock-in detection gives a lower SNR partly because of the unipolar laser intensity modulation. Half the laser power is used to maintain a proper bias for the laser power. This unmodulated laser power does not contribute to the measurement but adds shot noise to the receiver. Since the noise levels for both the on-line or off-line channels are determined by the photon shot noise from the total signal, the other channel adds to the shot noise.

4. Receiver SNR comparison–Experiments

We conducted laboratory experiments to test the derivations given above for the sine-wave and pulsed modulation direct detection receivers when operating under similar conditions. We did not conduct experiments for the coherent case, since the theory for it is well established.

4.1. Experiment for sine-wave modulation

We used a laser diode emitting at 1060 nm for the laser transmitter. The laser diode current was directly modulated by an arbitrary waveform generator, which could produce either sine-wave or pulsed waveforms. We used a near infrared photomultiplier tube (PMT) in photon counting mode as the detector. The choices of the laser wavelength and detector were for convenience since they were already set up in the lab, but the results should apply to the IPDA lidar techniques at other wavelengths.

For sine-wave modulation and lock-in detection, the test setup was configured exactly as that shown in Fig. 3. The laser was intensity modulated by injecting a bias current with the sum of two equal amplitude sine-wave signals at 50 kHz and 51 kHz, respectively. The laser diode output was coupled into a multimode optical fiber and the average power was monitored by an optical power meter and adjusted by a programmable optical fiber attenuator. An incandescent light bulb powered by a DC power supply was used to simulate the solar background light and was combined with the laser signal via a 2 to 1 optical fiber combiner. The amplitudes of the two sine-wave signals were kept the same as modeled in the theory given in the previous section.

The PMT at the receiver was operated in single photon counting mode. A fast discriminator was used to detect single photon events from the PMT and convert them into a pulse train of the standard shape with the leading edge of the pulse corresponded to the photon arrival time. The discriminator output then was passed through a BPF with a pass-band from 46 to 56 kHz. This electrical BPF was necessary to avoid aliasing in the subsequent analog-to-digital conversion and signal processing. The signal was digitized and recorded at 1 MHz sample rate with the use of a digitizing oscilloscope.

The signal induced shot noise from the on-line signal affected the noise floor for the off-line signal and vice versa. The rest of the signal processing was carried out by software in a personal computer (PC). The two LPFs used before the amplitude computation were 9-pole Bessel designs with a 5 Hz 3-dB bandwidth. The sampling interval between measurements was 0.2 seconds. These parameter values are summarized in Table 1.

4.2. Experiment for pulsed modulation

For the pulsed modulation and detection experiment, the same transmitter laser diode and detector were used. Here the laser diode was modulated with a pulse train with 1- μ sec wide rectangular pulses and a 10 kHz pulse rate. The PMT output after the discriminator was sent to a multichannel scaler (MCS). The MCS gives a histogram of the detected photons with a time span to include a pair of pulses, one for on-line signal and one off-line signal. The parameter values used in the experiments are also listed in Table 1. In post collection data analysis, the average numbers of detected signal photons was obtained by summing the photon counts over the intervals containing the laser pulses. The average rate of detected background photons and PMT dark counts was estimated by summing the counts over a given

interval between the pulses. The receiver SNR was calculated from the mean and standard deviation from 100 repeated measurements.

Table 1. Experiment Parameters

Laser Transmitter	1060 nm laser diode, intensity modulated by an arbitrary waveform generator (TEK AW2041)
<i>Sine-wave modulation:</i>	
Subcarrier frequencies	50 kHz on-line; 51 kHz off-line
Bandpass filter before digitizer	45 to 56 KHz (to prevent anti-aliasing)
Receiver lowpass filter bandwidth	5 Hz, 9 pole Bessel design
Digitizer sample rate	1 MHz
<i>Pulsed Modulation:</i>	
Pulse width	1 μ sec, rectangular shape
Pulse rate	10 KHz, alternating between on-line and off-line
Photon counting histogrammer	12.8 nsec range bin, 200 μ sec (15Kbins) per sweep and 0.2 sec (1000 sweeps) integration time
Detector	Hamamatsu H10330-75 PMT in photon counting mode

4.3. Results

Figure 6 shows measured SNR as a function of the average detected number of signal photons from the laboratory measurements of the sine-wave modulation lock-in detection technique and the pulsed modulation and detection technique. The solid lines show the results from theory based on the equations in the previous sections. The measurements agree well with the theory except at very high photon count rates where the receiver response appears to approach saturation.

As predicted, the pulsed modulation gives higher receiver SNR at a given input signal level. For the same average input signal level and at high input signal levels, the receiver SNR for the pulse modulation is $2\sqrt{2}$ times that of sine-wave modulation. To achieve the same SNR, the sine-wave modulation technique requires roughly 10 times the average signal power of pulsed modulation. These differences become larger when the background is high due to the noise reduction from the range gating in the pulsed receiver.

5. Conclusions

We have adapted theoretical models to calculate the receiver SNR vs. average number of detected signal photons for three different techniques for IPDA lidar: CW coherent detection and sine-wave and pulse modulated direct detections. We have also conducted laboratory experiments for the direct detection cases and the results agreed with theory. Coherent IPDA lidar have the advantages of high signal gain and narrow receiver optical bandwidth which can override the effect of the solar background light and detector noise. However, the measurement performance is limited in practice by the coherent mixing efficiency, speckle, and other effects. A direct detection lidar with sine-wave modulation can use a quasi-CW laser transmitter and synchronous detection. Measurements using low duty cycle pulsed laser modulation and time resolved averaging requires high laser peak power but is more efficient in terms of average received laser signal power to achieve the same receiver SNR. For high input signal levels, the receiver SNR for pulse modulation technique is $2\sqrt{2}$ times that of sine-wave modulation technique for the same average detected signal. The sine-wave modulation technique requires roughly 10 times the average signal of pulsed modulation technique to achieve the same SNR. These differences become larger at higher solar background levels due to the noise reduction from the range gating in the pulsed receiver.

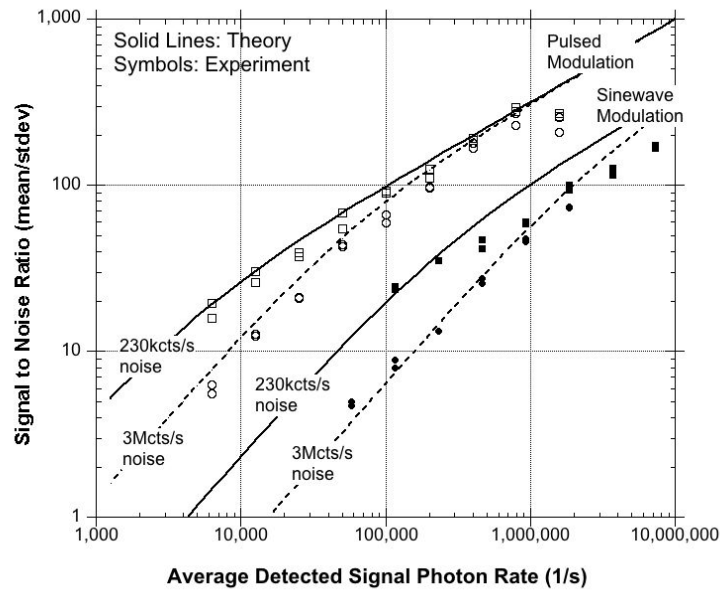


Fig. 6. Receiver SNR vs. the average detected number of signal photons from the laboratory tests of the sine-wave modulation with lock-in detection technique and the pulsed modulation and direct detection technique under detector dark noise only and $3e6/s$ detected background photons. The solid and dashed curves are the theoretical predictions based on the equations given in Section 3. The experimental data agreed well with the theory except at high signal photon count rate, likely due to the onset of receiver saturation. The system parameters of the experiments and the theoretical analysis are given in Table 1.

Acknowledgments

This work was supported by the NASA Earth Science Technology Office (ESTO) Instrument Incubator Program (IIP). We appreciate the helpful suggestions by the reviewers.